Journal of Electromagnetic Waves and Applications, Vol. 13, 923–941, 1999

RADIATION AND RECEIVING CHARACTERISTICS OF PARALLEL PLATE-FED SLOT ANTENNAS LOADED BY A DIELECTRIC CYLINDER: TM-CASE

J. L. Tsalamengas and G. Veronis

Department of Electrical and Computer Engineering
National Technical University of Athens
9 Iroon Polytechniou Str., GR-15773
Athens, Greece

Abstract–An exact analysis is presented for investigating parallel plate-fed slot antennas loaded by a dielectric cylinder. The primary excitation is taken to be either a TM incident mode of the parallel-plate waveguide or an incident H-polarized plane wave. The analysis combines singular integral equations with separation of variables techniques. The resulting integral equations are discretized using quasi-analytical methods, which lead to computationally efficient expressions for all matrix elements. This, in conjunction with the small matrix sizes required, leads to very accurate results with low computational cost. The numerical results presented reveal the effect of the load on the characteristics of the antennas.

1. INTRODUCTION

Dielectrically loaded waveguide radiators are widely used either in flush-mounted antennas or as radiating elements in phased arrays [1]. In this context, the parallel plate-fed slot antenna radiating into a dielectric half-space has been treated in [2] for the case of dominant (TEM) mode excitation of the formed symmetric iris. This same structure loaded by a dielectric semicylinder has been recently studied in [3] both for TM and for TE incident mode excitations.

In this work we study parallel plate-fed slot antennas loaded by a circular dielectric cylinder. The primary excitation is either a TM incident mode of the parallel-plate waveguide or an incident H-polarized plane wave. It should be noted that the formulation technique, followed

in [3] for the case of a semicylindrical dielectric load which resides right on the ground plane, is no longer applicable here.

The analysis conducted in section 2 leads to singular integral equations of the first kind. Discretization of these integral equations with the help of quasi-analytical techniques, yields for all matrix elements either closed form or rapidly converging series expressions. Because of this and the small matrix sizes required, very accurate results are obtained with low computational cost. The validation of the algorithms is carried out in section 3 followed by typical numerical results for several practical quantities of the structure. These results reveal how, by properly selecting the geometrical and physical parameters of the load, both the radiation and receiving efficiency of the antenna can be radically improved.

2. FORMULATION

The geometry of the problem is shown in Fig. 1. The slot of width $2w$ may be off-centered (i.e., $0 < c < \alpha$). The position of the cylinder of radius R is specified via the quantities (D, Φ). Regions **a** ($z < 0$), **1** ($\rho < R$) and **0** ($z > 0, \rho > R$), where ρ is measured from the center of the cylinder as in Fig. 2, are characterized by the scalars $(\varepsilon_i,\ \mu_i,\ k_i = \omega\sqrt{\varepsilon_i\mu_i})(i \equiv a, 1, 0)$.

The case of an incident TM-mode will be first treated in section 2.A. Latter on (section 2.B) we will consider an incident H-polarized plane wave excitation. In both cases, all electromagnetic fields involved in the analysis (for instance: incident field, excitation field, scattered field, total field; see below) have the form $(\overline{E} = \hat{x}E_x + \hat{z}E_z,\ \overline{H} = \hat{y}H_y)$, and are derivable from the single scalar H_y via relations of the form

$$E_x = -\frac{1}{j\omega\varepsilon}\frac{\partial H_y}{\partial z}, \qquad E_z = \frac{1}{j\omega\varepsilon}\frac{\partial H_y}{\partial x}. \tag{1}$$

In (1), ε is the permittivity at the observation point. The $\exp(+j\omega t)$ time dependence, assumed for all field quantities, is suppressed throughout the analysis that follows.

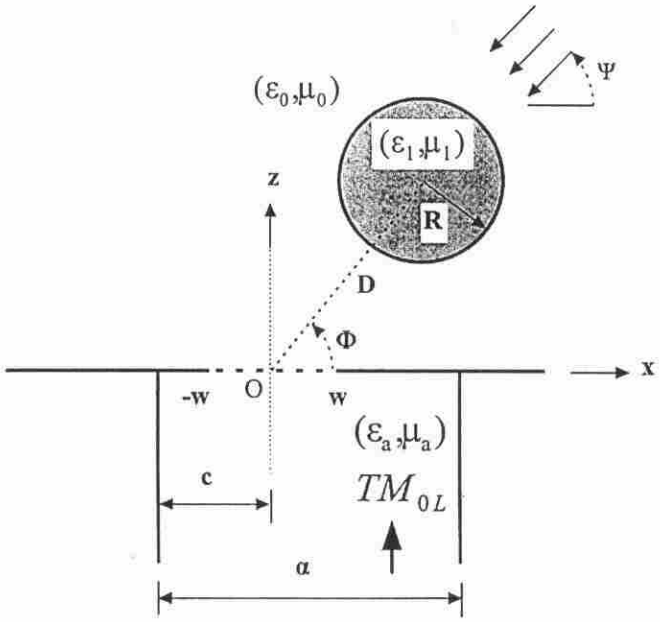

Figure 1. Geometry of the problem.

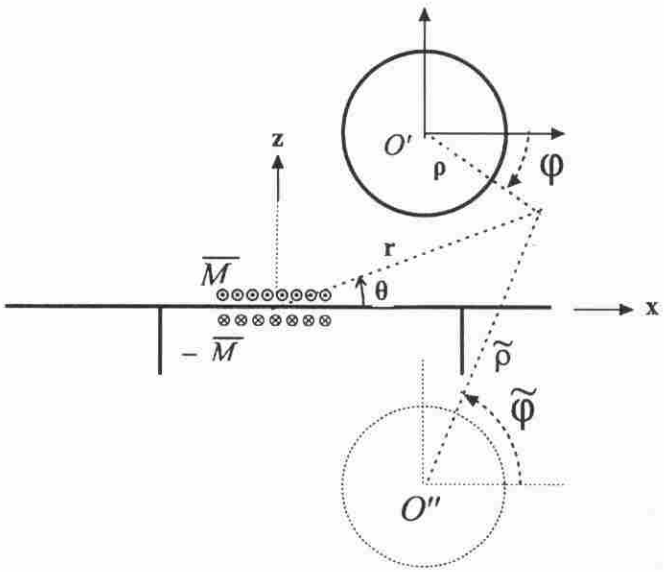

Figure 2. Equivalent problems for $z > 0$ and $z < 0$.

2.A Incident TM-mode Primary Excitation

Let the TM_{0L} mode be incident from below. The magnetic field of this mode is given by

$$\begin{aligned} &H_y^{inc}(x,z) = H_0\psi_L(x)e^{-\gamma_L z/\alpha}, \quad \psi_L(x) = \cos\left(L\pi\frac{x+c}{\alpha}\right), \\ &\gamma_L = \left[(L\pi)^2 - (k_a\alpha)^2\right]^{1/2}, \qquad 0 \le arg(\gamma_L) \le \frac{\pi}{2} \end{aligned} \tag{2}$$

Excitation Field : The field $(\overline{E}^{exc}, \overline{H}^{exc} = \hat{y}H_y^{exc})$ excited by the incident TM-mode when the slot is absent (short-circuited) will be termed "*excitation field*". Its magnetic field is given by

$$H_y^{exc}(x,z) = 2H_0\cosh(\gamma_L z/\alpha)\psi_L(x) \quad (z<0),\ 0\ (z>0) \tag{3}$$

Scattered field : The scattered field will be defined as the difference $(\overline{E},\overline{H}) = \left(\overline{E}^{tot},\overline{H}^{tot}\right) - \left(\overline{E}^{exc},\overline{H}^{exc}\right)$ between the total and the excitation field.

2.A.1 Representation of the Scattered Magnetic Field in Regions a, 0, 1

Invoking field equivalence principles, the formulation of the boundary value problem will be carried out in the way illustrated in Fig. 2 in terms of the equivalent surface magnetic currents $\pm\overline{M}(x)$, defined by

$$\overline{M}(x) = \overline{E}^{tot}(x,0)\times\hat{z} = -\hat{y}E_x(x,0) = \hat{y}M_y(x) \tag{4}$$

and radiating in the presence of a completely opaque ground plane at $z=0$.

Region a : Using a Green's function approach [3] , one obtains for the scattered magnetic field in region a the expression :

$$\begin{aligned} &H_y^{(a)}(x,z) = \int_{-w}^{w} M_y(x')G(z;x,x')dx' \\ &G(z;x,x') \equiv \omega\varepsilon_a\left[\frac{1}{k_a\alpha}e^{jk_a z} + 2j\sum_{n=1}^{\infty}\frac{1}{\gamma_n}\psi_n(x)\psi_n(x')e^{\frac{\gamma_n}{\alpha}z}\right] \end{aligned} \tag{5}$$

from which $\overline{E}^{(a)}(x,z)$ may be derived, if desired, via relations of the form (1).

Region 0 : The scattered field $\left(\overline{E}^{(0)}, \overline{H}^{(0)}\right)$ in region **0** may be written as superposition of two terms, denoted below by the superscripts s and c:

$$\left(\overline{E}^{(0)}, \overline{H}^{(0)}\right) \equiv \left(\overline{E}^{s}, \overline{H}^{s}\right) + \left(\overline{E}^{c}, \overline{H}^{c}\right). \tag{6}$$

These terms may be considered, respectively, as the fields originating from the slot (surface magnetic current $\overline{M}$) and from the cylinder (equivalent polarization currents), both acting in the presence of an infinite ground plane at $z = 0$.

For H_y^s one obtains the expression [4]

$$H_y^s(x,z) = -\frac{\omega\varepsilon_0}{2}\int_{-w}^{w} M_y(x') H_0^{(2)}\left(k_0\sqrt{(x-x')^2+z^2}\right) dx' \tag{7}$$

where $H_0^{(2)}(.)$ stands for the zero order Hankel function of the second kind. On the other hand, separation of variables yields for H_y^c the relation

$$H_y^c(x,z) = \sum_{n=-\infty}^{\infty} b_n \left[H_n^{(2)}(k_0\rho)e^{jn\varphi} + H_n^{(2)}(k_0\tilde{\rho})e^{-jn\tilde{\varphi}}\right] \tag{8}$$

where b_n are unknown expansion constants. In (8), (ρ, φ) and $(\tilde{\rho}, \tilde{\varphi})$, referring to the polar coordinate systems centered at O' and O'' respectively, are defined as in Fig. 2. (O'' is the image of O' with respect to the plane $z = 0$). The components of the electric field $\overline{E}^{(0)}$ are simple derivatives of $H_y^{(0)}$ (see (1)). [Note: Obviously, H_y^c is an even function of z. This, in view of the first of (1), implies that E_x^c is odd in z. Therefore, E_x^c vanishes at $z = 0$ as expected.]

Region 1 : The magnetic field in region **1** is given by:

$$H_y^{(1)} = \sum_{n=-\infty}^{\infty} c_n J_n(k_1\rho)e^{jn\varphi} \tag{9}$$

where c_n are unknown expansion constants. In terms of $H_y^{(1)}$ the electric field $\overline{E}^{(1)}$ may be derived using (1).

2.A.2 Integral Equations of the Problem

We note that, by having $+\overline{M}$ radiate into region $z > 0$ and $-\overline{M}$ radiate into region a, the continuity of the tangential electric field

E_x at $z = 0$ is automatically satisfied. The remaining boundary conditions of the problem: $H_y^{exc}(x,0-)+H_y^{(a)}(x,0) = H_y^{(0)}(x,0)$ $(|x| \leq w)$; $H_y^{(0)} = H_y^{(1)}$, $E_\varphi^{(0)} = E_\varphi^{(1)}$ $(\rho = R,\ 0 \leq \varphi \leq 2\pi)$ lead with the help of (2)–(9) to the following three integral equations:

$$\int_{-w}^{w} M_y(x') \left[-\frac{\omega\varepsilon_0}{2} H_0^{(2)}(k_0|x-x'|) - G(0;x,x') \right] dx'$$
$$+ 2 \sum_{n=-\infty}^{\infty} b_n \left[H_n^{(2)}(k_0\rho) e^{jn\varphi} \right]_{z=0} = H_y^{exc}(x,0-), \quad |x| \leq w \tag{10}$$

$$- \frac{\omega\varepsilon_0}{2} \int_{-w}^{w} M_y(x') H_0^{(2)} \left(k_0 \sqrt{(x-x')^2 + z^2} \right)_{\rho=R} dx'$$
$$+ \sum_{n=-\infty}^{\infty} b_n \left[H_n^{(2)}(k_0 R) e^{jn\varphi} + Q(R,\varphi) \right] - \sum_{n=-\infty}^{\infty} c_n J_n(k_1 R) e^{jn\varphi} = 0$$
$$0 \leq \varphi \leq 2\pi \tag{11}$$

$$- \frac{\omega}{2} \int_{-w}^{w} M_y(x') \frac{\partial}{\partial\rho} \left[H_0^{(2)} \left(k_0 \sqrt{(x-x')^2 + z^2} \right) \right]_{\rho=R} dx'$$
$$+ \frac{1}{\varepsilon_0} \sum_{n=-\infty}^{\infty} b_n \left[k_0 H_n'^{(2)}(k_0 R) e^{jn\varphi} + \frac{dQ(R,\varphi)}{dR} \right]$$
$$- \frac{k_1}{\varepsilon_1} \sum_{n=-\infty}^{\infty} c_n J_n'(k_1 R) e^{jn\varphi} = 0, \quad 0 \leq \varphi \leq 2\pi \tag{12}$$

where $J_n(.)$ stands for the Bessel function of order n whereas J_n' and H_n' denote derivatives with respect to argument. In (11)–(12), Q stands for the shorthand notation

$$Q(R,\varphi) \equiv H_n^{(2)}\ (k_0\tilde{\rho}) e^{-jn\tilde{\varphi}} \Big|_{\rho=R}$$
$$= \sum_{m=-\infty}^{\infty} H_{n-m}^{(2)}(2k_0 D \sin\Phi) J_m(k_0 R) e^{-jm\varphi} j^{m-n}. \tag{13}$$

The series expansion (13), based on the addition theorem for Hankel functions [5], is valid for any choice of the geometrical parameters of the structure.

In view of the edge condition, the unknown surface magnetic current $M_y(x)$ will be sought in the form:

$$M_y(x) = M_y[x(t)] = \frac{1}{\sqrt{1-t^2}} \sum_{N=0}^{\infty} a_N T_N(t); \quad t \equiv x/w \tag{14}$$

where a_N are expansion constants and T_N denote the Chebyshev polynomials of the first kind.

The unknown expansion coefficients a_N, b_n, c_n will be found from the integral equations (10)–(12) after inversion as outlined below.

2.A.3 Discretization of the Integral Equations

Equation (10): Let $x = wt$, $x' = wt'$ $(-1 \leq t, t' \leq 1)$. Inserting (14) into (10), multiplying both sides by $T_M(t)/\sqrt{1-t^2}$ and integrating from $t = -1$ to $t = 1$ yields the linear algebraic equations:

$$\sum_{N=0}^{\infty} a_N A_{MN}^{11} + \sum_{n=-\infty}^{\infty} b_n A_{Mn}^{12} = D_M^1, \qquad M = 0, 1, 2, \ldots \tag{15}$$

where

$$D_M^1 = \pi H_0 j^M c_M(L) \tag{16}$$

$$c_M(L) = \left[e^{jL\pi c/\alpha} + (-1)^M e^{-jL\pi c/\alpha}\right] J_M(L\pi w/\alpha). \tag{17}$$

Evaluation of A_{MN}^{11}

The matrix elements A_{MN}^{11} are given by

$$A_{MN}^{11} = \frac{jw\omega\varepsilon_0}{\pi} K_{MN}(k_0 w) + \omega K_{MN}^{\alpha}. \tag{18}$$

Here

$$K_{MN}(k_0 w) \equiv \frac{\pi j}{2} \int_{-1}^{1} dt \frac{T_M(t)}{\sqrt{1-t^2}} \int_{-1}^{1} dt' \frac{T_N(t')}{\sqrt{1-t'^2}} H_0^{(2)}(k_0 w|t-t'|) \tag{19}$$

is identified with $K_{MN}(k_0 w) = K_{MN}^{s}(k_0 w) + K_{MN}^{\tau}(k_0 w)$ of [6] where K_{MN}^{s} and K_{MN}^{τ} assume extremely efficient analytical expressions (see equations (19)–(20) of [6]). On the other hand

$$K_{MN}^{a} = -\pi^2 w \varepsilon_a \left[\frac{1}{k_a \alpha} \delta_{M0}\delta_{N0} + j^{M+N+1} S_{MN}^{a}\right] \tag{20a}$$

where δ_{nm} stands for Kronecker delta, whereas

$$S_{MN}^{a} = \sum_{n=1}^{\infty} \frac{1}{\gamma_n} J_M(n\pi w/\alpha) J_N(n\pi w/\alpha) f_{MN}(n) \tag{20b}$$

$$f_{MN}(n) = \begin{cases} (-1)^M + \cos(2n\pi c/\alpha), & (M+N \text{ even}) \\ j\sin(2n\pi c/\alpha), & (M+N \text{ odd}). \end{cases} \tag{20c}$$

S^a_{MN}, which converges as n^{-2} (i.e., rather slowly), can be accelerated to any order by several powerful techniques explored in [3]. Using its accelerated form (see section 3 of [3]), S^a_{MN} requires no more than 10–20 terms in order to achieve an accuracy to within at least 14 significant figures.

Evaluation of A^{12}_{Mn}

$$A^{12}_{Mn} \equiv 2\int_{-1}^{1} \frac{T_M(t)}{\sqrt{1-t^2}} \left[H^{(2)}_n(k_0\rho)e^{jn\varphi}\right]_{z=0} dt \tag{21}$$

can be efficiently evaluated in the way outlined below.

a. **w < D case :** In this case the following expansion

$$H^{(2)}_n(k_0\rho)\, e^{jn\varphi}\big|_{z=0} = \sum_{m=-\infty}^{\infty} H^{(2)}_{n-m}(k_0D)J_m(k_0x)(-1)^{n-m}e^{j(n-m)\Phi}, \tag{22}$$

based on the addition theorem for Hankel functions, is valid. Substituting (22) into (21) and carrying out the integration involved one obtains:

$$A^{12}_{Mn} = 2\sum_{m=-\infty}^{\infty} H^{(2)}_{n-m}(k_0D)e^{j(n-m)(\pi+\Phi)}I(M,m;k_0w) \tag{23a}$$

$$= \sum_{m=0}^{\infty}(2-\delta_{m0})\left[H^{(2)}_{n-m}(k_0D)e^{j(n-m)(\pi+\Phi)} + (-1)^m H^{(2)}_{n+m}(k_0D)e^{j(n+m)(\pi+\Phi)}\right] I(M,m;k_0w) \tag{23b}$$

with

$$I(p,q,k_0w) \equiv \int_{-1}^{1} \frac{T_p(t')}{\sqrt{1-t'^2}} J_q(k_0wt')dt' = \pi \begin{cases} J_{\frac{p+q}{2}}(k_0w/2)J_{\frac{q-p}{2}}(k_0w/2), & p+q \text{ even} \\ 0, & p+q \text{ odd.} \end{cases} \tag{23c}$$

b. **General case :** When $w > D$, expansion (22) is no longer applicable due to well known limitations inherent to the addition theorem for Hankel functions. An alternative efficient method to evaluate A^{12}_{Mn}, free of any limitations, is based on Lobatto's summation formula [5]:

$$\int_{-1}^{1} \frac{f(t)}{\sqrt{1-t^2}} dt = \frac{\pi}{m} \sum_{i=1}^{m} f(t_i), \qquad t_i = \cos \frac{(2i-1)\pi}{2m} \tag{24}$$

where the fixed integer m is selected as high as needed to achieve any prescribed accuracy. Using (24) as well as the relation $T_M(\cos\theta) = \cos(M\theta)$ one ends up with the result:

$$A_{Mn}^{12} = \frac{2\pi}{m} \sum_{i=1}^{m} \cos\left[\frac{(2i-1)M\pi}{2m}\right] \cdot H_n^{(2)}\left(k_0\sqrt{w^2t_i^2 - 2wt_iD\cos\Phi + D^2}\right) e^{jn\varphi(t_i)} \tag{25}$$

where

$$\varphi(t) = \tan^{-1}(-D\sin\Phi, wt - D\cos\Phi). \tag{26}$$

The function $\tan^{-1}(y,x)$ is implemented by the DATAN2(Y,X) routine of FORTRAN.

Note: Expression (25) is quite general, valid both for $w \geq D$ and $w < D$. In the latter case $(w < D)$ it provides an independent test of the correctness of (23a–b) (see section 3).

Equation (11): Inserting (14) into (11), multiplying both sides by $e^{-jM\varphi}/(2\pi)$, and integrating from $\varphi = 0$ to $\varphi = 2\pi$ we obtain the algebraic equations

$$\sum_{N=0}^{\infty} a_N A_{MN}^{21} + \sum_{n=-\infty}^{\infty} b_n A_{Mn}^{22} + \sum_{n=-\infty}^{\infty} c_n A_{Mn}^{23} = D_M^2, \quad M = 0, \pm 1, \pm 2, \ldots \tag{27}$$

where

$$D_M^2 = 0 \tag{28}$$

The matrix elements A_{Mn}^{22} and A_{Mn}^{23} assume the closed form expressions

$$A_{Mn}^{22} = H_{n+M}^{(2)}(2k_0D\sin\Phi) J_M(k_0R) j^{n+M}(-1)^n + H_M^{(2)}(k_0R)\delta_{nM} \tag{29}$$

$$A_{Mn}^{23} = -J_M(k_1R)\delta_{nM}. \tag{30}$$

Evaluation of A_{MN}^{21}

$$A_{MN}^{21} \equiv -\frac{\omega w \varepsilon_0}{4\pi} \int_{-1}^{1} dt' \frac{T_N(t')}{\sqrt{1-t'^2}} \int_0^{2\pi} H_0^{(2)}\left(k_0\sqrt{(x-x')^2+z^2}\right)_{\rho=R} e^{-jM\varphi} d\varphi \tag{31}$$

will be evaluated as follows.

$\mathbf{w < D - R}$ case : In this case the expansion

$$\begin{aligned} &H_0^{(2)}\left(k_0\sqrt{(x-x')^2+z^2}\right)_{\rho=R} \\ &= \sum_{m=-\infty}^{\infty} H_m^{(2)}(k_0 r) J_m(k_0 x') e^{jm\theta}\Big|_{\rho=R} \\ &= \sum_{m=-\infty}^{\infty} J_m(k_0 x') \sum_{k=-\infty}^{\infty} H_{m-k}^{(2)}(k_0 D) J_k(k_0 R) e^{jk\varphi} e^{j(m-k)\Phi} \end{aligned} \tag{32}$$

is valid, leading to the result:

$$A_{MN}^{21} = \frac{-\omega w \varepsilon_0}{2} J_M(k_0 R) V_{MN} \tag{33a}$$

$$V_{MN} = \sum_{m=-\infty}^{\infty} I(N, m; k_0 w) H_{m-M}^{(2)}(k_0 D) e^{j(m-M)\Phi}. \tag{33b}$$

General case : When $w > D - R$, (32) is no longer applicable. A general method to evaluate A_{MN}^{21}, free of any limitations (i.e., valid for $w > D - R$ as well as for $w \le D - R$), is based on formula (24) and the expansion:

$$\begin{aligned} &H_0^{(2)}\left(k_0\sqrt{(x-x')^2+z^2}\right)\Big|_{\rho=R} \\ &= \sum_{m=-\infty}^{\infty} H_m^{(2)}(k_0 d_1) J_m(k_0 R) e^{jm\varphi} e^{jm(\pi-\theta_1)} \end{aligned} \tag{34}$$

where

$$d_1 = \sqrt{(D\cos\Phi - x')^2 + (D\sin\Phi)^2} = \sqrt{x'^2 - 2x'D\cos\Phi + D^2} \tag{35a}$$

$$\theta_1 = \tan^{-1}(D\sin\Phi, D\cos\Phi - x') = \theta_1(t') \quad (t' \equiv x'/w). \tag{35b}$$

The sought expression then results in the form

$$A_{MN}^{21} = -\frac{\omega w \varepsilon_0}{2} J_M(k_0 R) G_{MN} \tag{36a}$$

$$G_{MN} = \frac{\pi}{m} \sum_{i=1}^{m} \cos\left[\frac{(2i-1)N\pi}{2m}\right] H_M^{(2)}\left(k_0 \sqrt{w^2 t_i^2 - 2wt_i D \cos\Phi + D^2}\right) e^{jM(\pi - \theta_1(t_i))} \tag{36b}$$

with t_i defined in (24).

Equation (12) : This equation is analogous to (11) and can thus be treated in the same way, leading to the linear algebraic equations of

$$\sum_{N=0}^{\infty} a_N A_{MN}^{31} + \sum_{n=-\infty}^{\infty} b_n A_{Mn}^{32} + \sum_{n=-\infty}^{\infty} c_n A_{Mn}^{33} = D_M^3, \quad M = 0, \pm 1, \pm 2, \ldots \tag{37}$$

where

$$D_M^3 = 0 \tag{38}$$

In (37) A_{Mn}^{32} and A_{Mn}^{33} assume the closed form expressions:

$$A_{Mn}^{32} = \frac{k_0}{\varepsilon_0}\left[H_{n+M}^{(2)}(2k_0 D \sin\Phi) J'_M(k_0 R) j^{n+M}(-1)^n + H_M'^{(2)}(k_0 R)\delta_{nM}\right] \tag{39}$$

$$A_{Mn}^{33} = -\frac{k_1}{\varepsilon_1} J'_M(k_1 R)\delta_{nM}. \tag{40}$$

Finally, A_{Mn}^{31} takes either the expression

$$A_{MN}^{31} = -\frac{\omega w k_0}{2} J'_M(k_0 R) V_{MN} \tag{41a}$$

with V_{MN} defined in (33b), or the expression

$$A_{MN}^{31} = -\frac{\omega w k_0}{2} J'_M(k_0 R) G_{MN} \tag{41b}$$

with G_{MN} defined in (36b). Equation (41a) is subject on the restriction $w < D - R$ whereas (41b) has no limitation.

The unknown expansion coefficients are determined from the system of (15), (27), (37) after truncation and inversion. In terms of these

coefficients any quantity of practical interest (such as near and far radiated fields, reflection coefficients etc.) may be found as explained in section 3.

2.B H-Polarized Plane Wave Excitation

Let us now consider the following H-polarized plane wave

$$\begin{aligned} &\overline{H}^{inc} = \hat{y} H_0 e^{-jk_0 \hat{k}_{inc}\cdot\bar{r}}, \qquad \overline{E}^{inc} = -Z_0 \hat{k}_{inc} \times \overline{H}^{inc}, \\ &Z_0 = \sqrt{\mu_0/\varepsilon_0}, \qquad \hat{k}_{inc} = -\hat{x}\cos\psi - \hat{z}\sin\psi, \qquad \bar{r} = x\hat{x} + z\hat{z} \end{aligned} \tag{42}$$

be incident from region **0**. In this case, we will define the "excitation field" as the field excited by the incident wave, in the absence of the cylinder, when the slot is short-circuited. Its magnetic field is given by

$$H_y^{exc}(x,z) = 2H_0 e^{jk_0 x\cos\psi}\cos(k_0 z\sin\psi) \quad (z>0),\ 0\ (z<0) \tag{43}$$

The scattered field in regions **a, 0, 1** is again expressible via (5), (6)–(8), (9).

The boundary conditions of the problem, $H_y^{(a)}(x,0) = H_y^{exc}(x,0+) + H_y^{(0)}(x,0)(|x| \le w)$; $H_y^{(0)} + H_y^{exc} = H_y^{(1)}$, $E_\varphi^{(0)} + E_\varphi^{exc} = E_\varphi^{(1)}(\rho = R,\ 0 \le \varphi < 2\pi)$ lead to three integral equations which are identical with those of (10), (11), (12) respectively with the following exceptions: **(a)** the right side term $H_y^{exc}(x,0-)$ in (10) is now replaced by $-H_y^{exc}(x,0+)$ given by (43), **(b)** the right side of (11) is $-H_y^{exc}(x,z)|_{\rho=R}$ instead of 0, **(c)** the right side of (12) is $-\frac{1}{\varepsilon_0}\frac{\partial}{\partial\rho} \cdot H_y^{exc}(x,z)|_{\rho=R}$.

Discretization of the above integral equations in the way outlined in the preceding section 2.A leads again to the linear system of equations (15), (27), (37) where the matrix elements retain their expressions derived in section 2.A. On the other hand, the excitation (constant) terms D_M^1, D_M^2, D_M^3 are now given by the relations

$$D_M^1 = -2H_0\pi j^M J_M(k_0 w\cos\psi), \qquad M = 0,1,2,\ldots \tag{44}$$

$$D_M^2 = -H_0 j^M J_M(k_0 R) F_M, \qquad M = 0,\pm1,\pm2,\ldots \tag{45}$$

$$D_M^3 = -\frac{k_0}{\varepsilon_0} H_0 j^M J_M'(k_0 R) F_M, \qquad M = 0,\pm1,\pm2,\ldots \tag{46}$$

$$F_M = e^{jk_0 D\cos(\Phi-\psi)} e^{-jM\psi} + e^{jk_0 D\cos(\Phi+\psi)} e^{jM\psi}. \tag{47}$$

2.C Scattered Fields

The scattered magnetic field inside region **a** is given by

$$H_y^{(a)}(x,z) = \sum_{n=0}^{\infty} T_{0n}^{TM} \psi_n(x) e^{\gamma_n z/\alpha} \tag{48}$$

where

$$T_{0n}^{TM} = \frac{\pi(2-\delta_{n0})}{2\gamma_n} w\omega\varepsilon_a \sum_{N=0}^{\infty} a_N j^{N+1} c_N(n) \tag{49}$$

(c_N is given by (17)).

In the case of the TM_{0L} incident mode (section 2.A) the reflection coefficient of this mode is given by

$$R_{0L}^{TM} = 1 + T_{0L}^{TM}. \tag{50}$$

The far scattered magnetic field in region **0** in polar coordinates (r,θ) and the per unit length far-scattered power are obtained from the relations

$$\begin{aligned} H_y^{(0)}(r,\theta) = &\sqrt{\frac{2}{\pi k_0 r}} \left(-\frac{\omega w \varepsilon_0}{2}\right) \sum_{N=0}^{\infty} a_N \sum_{m=0}^{\infty} (2-\delta_{m0}) I(N,m) \cos(m\theta) \\ &\cdot e^{-j(k_0 r - m\pi/2 - \pi/4)} + 2\sqrt{\frac{2}{\pi k_0 r}} \sum_{n=-\infty}^{\infty} b_n \sum_{m=-\infty}^{\infty} J_m(k_0 D) \\ &\cdot e^{jm(\pi+\Phi)} \cos[(n-m)\theta] e^{-j(k_0 r - (n-m)\pi/2 - \pi/4)} \end{aligned} \tag{51}$$

$$P_{rad} = \int_0^{\pi} r P_r d\theta = \frac{1}{2} Z_0 \int_0^{\pi} r |H_y^{(0)}|^2 d\theta. \tag{52}$$

3. NUMERICAL RESULTS AND DISCUSSION

Sample numerical results are presented below for the parameter values $\mu_\alpha = \mu_1 = \mu_0,\ \varepsilon_a = \varepsilon_0,\ c/\alpha = 0.5,\ w/\alpha = 0.25,\ H_0 = 1(A/m)$.

3.A Convergence of the Matrix Elements

Table 1 presents values of the leading matrix element A_{00}^{12} as obtained via (23b), using $m_{\max}$ series terms, and from (25) for several

values of m. The parameter values are $D = 0.4\lambda$, $w = 0.2\lambda$, $\Phi = \pi/2$ (λ =free-space wavelength). We see, e.g., that using $m_{\max} = 40$ series terms in (23b) or $m = 12$ in (25) suffices to obtain an accuracy to within 16 significant decimals. The convergence of other matrix elements is similar.

$m_{\max}$	A_{00}^{12} of equation (23b)
10	$-0.782764066828540 - j2.93042135312132$
20	$-0.782764066828540 - j2.93040407431706$
25	$-0.782764066828540 - j2.93040408036071$
30	$-0.782764066828540 - j2.93040408066939$
35	$-0.782764066828540 - j2.93040408066612$
40	$-0.782764066828540 - j2.93040408066593$
45	$-0.782764066828540 - j2.93040408066594$
$m_{\max}$	A_{00}^{12} of equation (25)
4	$-0.782765501666841 - j2.93042334847546$
6	$-0.782764066845851 - j2.93040410965371$
8	$-0.782764066828540 - j2.93040408072615$
10	$-0.782764066828540 - j2.93040408066608$
12	$-0.782764066828540 - j2.93040408066594$
14	$-0.782764066828540 - j2.93040408066594$

Table 1. Convergence of A_{00}^{12} for $D = 0.4\lambda$, $\Phi = \pi/2$, $w = 0.2\lambda$.

3.B Convergence and Validation of the Algorithms

The convergence characteristics of the algorithms will be illustrated in relation with the following truncated form of the linear algebraic system of equations (15), (27), and (37):

$$\sum_{N=0}^{N_1-1} a_N A_{MN}^{11} + \sum_{n=-N_2}^{N_2} b_n A_{Mn}^{12} = D_M^1,$$
$$M = 0, 1, 2, \ldots, N_1 - 1$$

$$\sum_{N=0}^{N_1-1} a_N A_{MN}^{21} + \sum_{n=-N_2}^{N_2} b_n A_{Mn}^{22} + \sum_{n=-N_2}^{N_2} c_n A_{Mn}^{23} = D_M^2,$$
$$M = 0, \pm 1, \pm 2, \ldots, \pm N_2$$
$$\sum_{N=0}^{N_1-1} a_N A_{MN}^{31} + \sum_{n=-N_2}^{N_2} b_n A_{Mn}^{32} + \sum_{n=-N_2}^{N_2} c_n A_{Mn}^{33} = D_M^3,$$
$$M = 0, \pm 1, \pm 2, \ldots, \pm N_2$$

The convergence versus truncation size is illustrated in Table 2 where the radiation efficiency P_{rad}/P_{inc} is shown for the TM_{00} incident mode when $\alpha = 0.4\lambda$, $D = \lambda$, $R = 0.3\lambda$, $\Phi = \pi/2$, $\varepsilon_r \equiv \varepsilon_1/\varepsilon_0 = 2$. As seen, the convergence is rapid and stable.

$N_1 = N_2$	P_{rad}/P_{inc}
5	0.7835181052573
10	0.7835183144093
20	0.7835183144092

Table 2. Convergence of P_{rad}/P_{inc} for the TM_{00} incident mode at $\alpha = 0.4\lambda$, $D = \lambda$, $R = 0.3\lambda$, $\Phi = \pi/2$, $\varepsilon_r = 2$.

In the case of a TM incident mode, a validity test that has been extensively used was based on energy conservation principle: $P_{inc} = P_{refl} + P_{rad}$. In the case of an incident plane wave primary excitation, the correctness of the algorithm was tested by verifying the validity of the relation $H_y^{(0)}(r, \theta = \theta_0; \psi = \psi_0) = H_y^{(0)}(r, \theta = \psi_0; \psi = \theta_0)$, based on the reciprocity theorem. In all numerous cases that have been considered both these relations were ascertained to within at least 13 significant decimals.

3.C Further Numerical Results

For the case of TM_{00} incident mode, Fig. 3 shows the radiation efficiency (P_{rad}/P_{inc}) versus D/λ, R/λ, ε_r, and α/λ. For the sake of comparisons, the case $\varepsilon_r = 1 \backslash R = 0$ (unloaded antenna) is also included. We observe that, for the parameter values selected, the unloaded antenna is a poor radiator over the entire frequency range. In

contrast, by properly selecting the geometrical and physical parameters of the load a very high efficiency is attainable. For instance, the choice $\alpha/\lambda = 0.8$, $R/\lambda = 0.3$, $D/\lambda = 0.4$, $\varepsilon_r = 6$ leads to an almost perfect matching $(P_{rad}/P_{inc} > 997/1000)$. This radical improvement in the radiation efficiency may be attributed to strong multiple reflections introduced by the loading. This resonance behaviour, suggested by the periodicity in all pertinent curves in Fig. 3a, is also exhibited by the normalized admittance $Y = G + jB = \left(1 + R_{00}^{TM}\right) / \left(1 - R_{00}^{TM}\right)$ as shown in Fig. 4 for $R = 3\alpha/8$, $\varepsilon_r = 6$, and for several values of D.

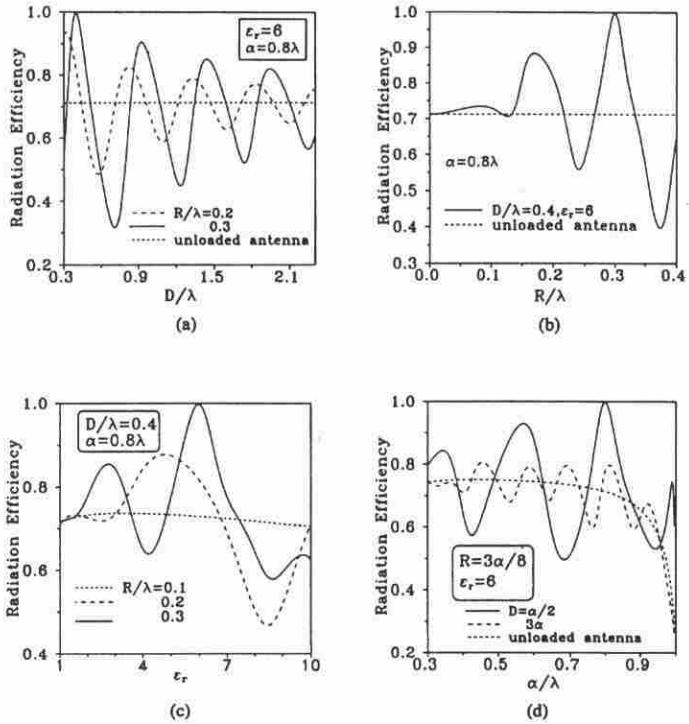

Figure 3. Radiation efficiency $(\frac{P_{rad}}{P_{inc}})$ versus (a) D/λ, (b) R/λ, (c) ε_r, (d) α/λ.

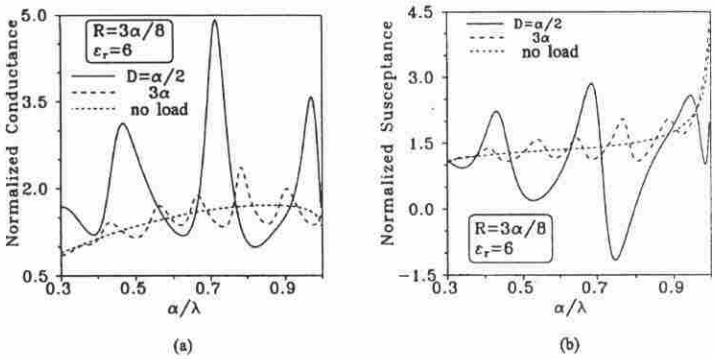

Figure 4. Normalized admittance $Y = G + jB$ versus α/λ for $R = 3\alpha/8$, $\varepsilon_r = 6$, and for several values of D. (a) G, (b) B.

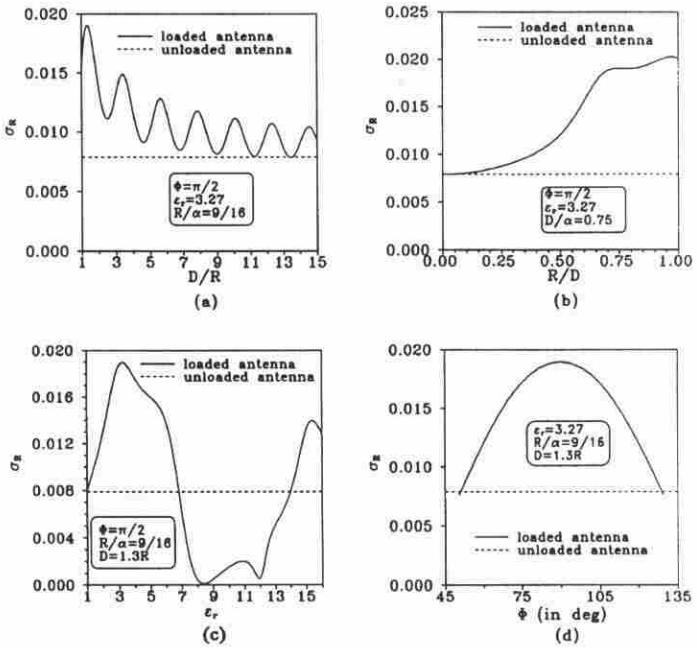

Figure 5. Receiving cross section σ_R versus (a) D, (b) R, (c) ε_r, (d) Φ for $\Psi = \pi/2$.

The receiving characteristics of the structure are illustrated in Fig. 5 in case of an incident plane wave for $f = 10\,\text{GHz}$, $\Psi = \pi/2$, $\alpha = 0.4\lambda$ (the other parameter values are shown in the insets). In this figure we show the per unit length receiving cross section (σ_R) as a function of D, R, ε_r, and Φ. The receiving cross section is defined by

$$\sigma_R = \frac{\textit{Power} \text{ received by the antenna}}{\textit{incident} \text{ power density}} = \frac{P_{rec}}{\frac{1}{2} Z_0 |H_0|^2}$$

where

$$P_{rec} = \sum_{n=0}^{N_{prop}} |T_{0n}^{TM}|^2 \frac{|\gamma_n|}{2(2-\delta_{n0})\omega\varepsilon_\alpha}$$

with T_{0n}^{TM} given by (49) and N_{prop} denoting the number of propagating waveguide modes. From these curves, where the case of the unloaded antenna is also included for comparison (dotted lines), we conclude again that by properly selecting the values of the geometrical parameters of the load the receiving efficiency may be radically improved.

4. CONCLUSION

Analytical methods have been used to analyze the parallel plate-fed slot antenna loaded with a dielectric cylinder. These techniques yield either closed form or rapidly converging series expressions for all matrix elements. Proper choice of the geometrical and physical parameters of the load results in a radical improvement in both the radiation and receiving efficiency of the antenna.

REFERENCES

1. Wu, C. P., "Integral equation solutions for the radiation from a waveguide through a dielectric slab," *IEEE Trans. Antennas Propagat.*, Vol. 17, 733–739, Nov. 1969.
2. Scharstein, R. W., "Two numerical solutions for the parallel plate-fed slot antenna," *IEEE Trans. Antennas Propagat.*, Vol. 37, 1415–1426, Nov. 1989.
3. Tsalamengas, J. L., "A parallel plate-fed slot antenna loaded by a dielectric semicylinder," *IEEE Trans. Antennas Propagat.*, Vol. 44, No. 7, 1031–1040, July 1996.

4. Tsalamengas, J. L., "TE/TM electromagnetic scattering by a slot on a ground plane and in the presence of a semi-cylindrical load," *JEWA,* Vol. 8, No. 5, 613–646, 1994.
5. Abramowitz, M., and I. A. Stegun, *Handbook of Mathematical Functions,* New York: Dover, 1972.
6. Tsalamengas, J. L., and J. G. Fikioris, "Efficient solutions for scattering from strips and slots in the presence of a dielectric half-space: Extension to wide scatterers -Part I: Theory," *J. Appl. Phys.,* Vol. 70(3), 1121–1131, Aug. 1991.

J. L. Tsalamengas was born in Karditsa, Greece, in 1953. He received the Diploma of Electrical and Mechanical Engineering and the doctor's degree in Electrical Engineering from the National Technical University of Athens (NTUA), Greece, in 1977 and 1983, respectively. Since November 1995 he has been a Professor of Electrical Engineering at the NTUA where he has been teaching since 1984. His fields of interest include problems of wave propagation, radiation and scattering in the presence of complex media, computation electromagnetic, and applied mathematics.

Georgios Veronis was born on January 11, 1975 in Athens, Greece. He received the B.S. degree in electrical engineering from the National Technical University of Athens in 1997. He is currently working toward the M.S. degree in electrical engineering at Stanford University. His research interests include computational electromagnetics, plasma physics and applications.